Structural properties and electronic structure of some ternary d-electron and f-electron intermetallics

2000 J. Phys.: Condens. Matter 12 1269

(http://iopscience.iop.org/0953-8984/12/7/311)

J. Phys.: Condens. Matter **12** (2000) 1269–1284. Printed in the UK PII: S0953-8984(00)07431-2

Structural properties and electronic structure of some ternary d-electron and f-electron intermetallics

A Ślebarski†, M Orzechowska†, A Wrona†, J Szade† and A Jezierski‡

† Institute of Physics, University of Silesia, 40-007 Katowice, Poland

‡ Institute of Molecular Physics, Polish Academy of Sciences, 60-179 Poznań, Poland

Received 13 August 1999, in final form 8 December 1999

Abstract. We report on structural measurements on and electronic structure investigations of the alloyed compounds ZrNiSn, TiNiSn, CeNiSn and CeRhSb. We present measurements of lattice parameters as a function of temperature and analysis of $a(T)$ and its relation to χT, χ being the magnetic susceptibility. We observed a linear dependence of $a(T)$ versus χT for Zr, Ti and Ce alloys (for orthorhombic Ce alloys, the lattice parameters a, b and c scale linearly with χT). The x-ray photoelectron and ultraviolet photoemission spectra are further compared to the density of states, obtained from band-structure calculations.

1. Introduction

Ce-based heavy-fermion metals, which are characterized by large Sommerfeld constants, exhibit various metallic ground states. Among strongly correlated f-electron systems there are a group of small-gap semiconductors which might be expected to be metallic, judging from the properties of their f-series analogues. These semiconductors are orthorhombic (CeNiSn [1, 2], CeRhSb [3]) or cubic ($Ce_3Bi_4Pd_3$ [4]) and their susceptibilities and lattice parameters indicate mixed-valence character of the f electron. These compounds can be regarded as highly renormalized band insulators, where the f electrons behave as valence electrons.

Recently, we have shown that the mixed valence of Ce in CeNiSn and CeRhSb seems to be correlated with the formation of a gap at the Fermi level [5]. In every case there is an isostructural semiconductor in which Ce is replaced by a tetravalent non-4f element, when the trivalent 4f analogues are metallic. In reference [6] we have argued for ZrNiSn and TiNiSn that the lowering of the valence of tetravalent Zr or Ti in the Ce-doped samples closes the gap at the Fermi level. Very similar band properties are well known for CeNiSn, which is considered a Kondo insulator.

Both MNiSn and CeNiSn are intermetallic and strongly hybridized materials. Previous alloying studies have shown that the energy gap in Ce-based Kondo insulators is unstable against change in the hybridization of the 4f conduction electrons. Replacing all of the Ce ions in a Kondo insulator with trivalent ions leads to an ordinary metallic state, whereas by replacing the Ce ions with tetravalent non-f-electron ions, such as Zr, Ti or Hf ions, a semiconducting state is obtained. Accordingly, the gap ($\sim$400 meV in ZrNiSn) is destroyed if Ni is replaced by another transition element, such as Co. This gap can also be suppressed by a partial substitution of a trivalent metal (e.g. Ce) for Zr^{4+}, despite the fact that the electronic structures of ZrNiSn and CeNiSn are rather simple and similar [7, 8]. We have also found that the gap is

0953-8984/00/071269+16$30.00

dependent on the local environment of the metal M for both compounds [5]. The electronic specific heat and the Hall effect for MNiSn compounds reveal a rather high effective mass for the current carriers m^*, of the order of 2–4 times the electron mass m_0 [9, 10].

The similar behaviour observed in MNiSn-type compounds with M = Zr, Ti and Hf or Ce motivated us to try to find the role of the M atom in the energy spectrum near the Fermi energy. Here, we attempt to classify the non-magnetic narrow-gap semiconductors MNiSn and the Ce Kondo insulators into a group of alloys with strong hybridization of the electronic states near the Fermi energy. Reported herein are the results of an investigation consisting of measurements of crystal structure, magnetization and both UP and XP valence band spectra.

2. Experimental procedure

The samples of CeNiSn, CeRhSb, ZrNiSn, TiNiSn and their alloys were arc melted on a cooled copper crucible in a high-purity argon atmosphere and remelted ten times, and then annealed at 800 °C for one week. The constituents were Specpure. The x-ray analysis showed single-phase samples within the usual resolution of 6%. The compounds were identified by their powder diagrams which were recorded using x-ray Debye–Sherrer powder diffraction with Cu Kα radiation using a Siemens D-5000 diffractometer. The lattice parameters were investigated as a function of temperature between 8 K and 300 K. The ultraviolet photoemission spectra (UPS), x-ray photoelectron spectra (XPS) and Auger spectra were taken with a Physical Electronics PHI 5700 ESCA spectrometer. He I and He II radiation was used in the UPS regime. The Auger transitions and the XP spectra were observed using monochromatized Al Kα radiation at room temperature. The vacuum during the Auger measurements was about 10^{-10} Torr, and it was 10^{-9} Torr when the helium lamp was used. The samples were scraped in an UHV with a diamond file. For some samples, sputtering with Ar ions was used to ensure that the surface was free from contamination. Then a low-energy ion beam (below 1 keV) was used and it was checked that the sputtering did not influence the chemical composition or the shape of the peaks. The level of oxygen and carbon contamination was controlled during the measurements. The UPS data were obtained within a short time to avoid the effects of oxygen deposition. Calibration of the spectra was performed according to reference [11]. Binding energies were referenced to the Fermi level ($\epsilon_F = 0$).

The electronic structures of the ordered alloys were studied by the self-consistent tight-binding linearized muffin-tin orbital method [12] within the atomic sphere approximation (ASA) and the local spin-density (LSD) approximation. The exchange–correlation potential was taken in the form proposed by von Barth and Hedin [13], and Langreth–Mehl–Hu (LMH) corrections were included [14]. In the band calculations we assumed the initial configurations to be according to the periodic table of elements. The electronic structures were computed for the experimental lattice parameters for the supercell model. The values of the atomic sphere radii were taken in such a way that the sum of all atomic sphere volumes was equal to the volume of the unit cell.

3. Results and discussion

3.1. Structural and magnetic properties

ZrNiSn has a MgAgAs-type structure and is a strongly disordered alloy because of the closeness of the Zr- and Sn-atom radii. These atoms may substitute for each other. Therefore, in reference [9] a chemical formula of the $Zr_{1-x}Sn_xNi(Vac)Sn_{1-x}Zr_x$ type and with $0.1 < x < 0.3$ was obtained for ZrNiSn in agreement with the x-ray diffraction analysis. In figure 1 we

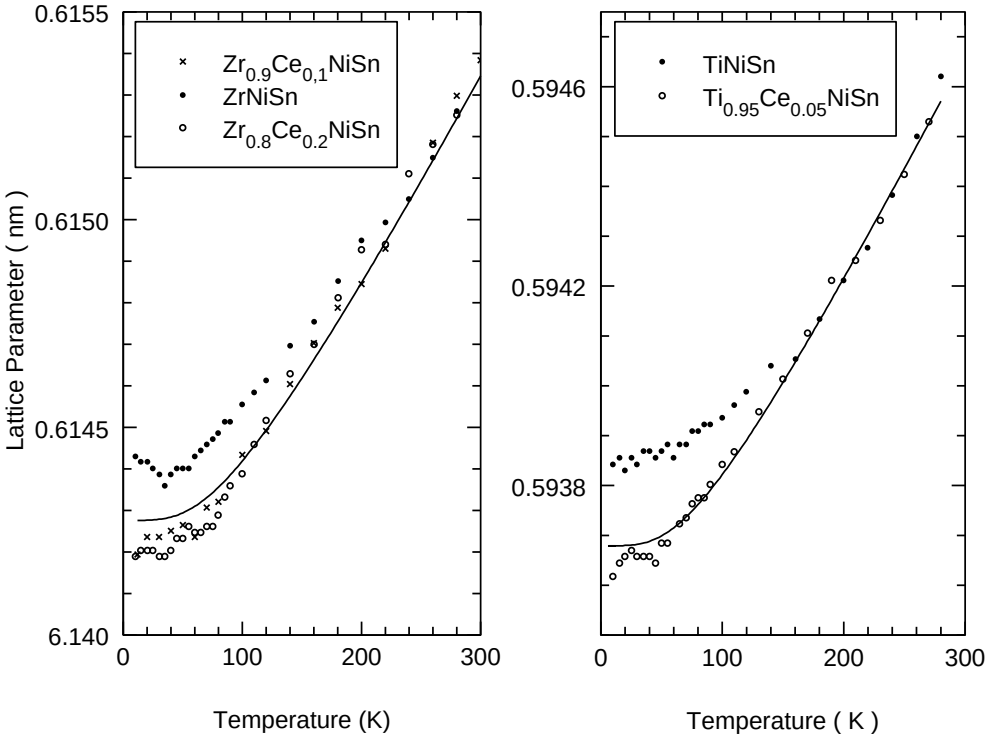

Figure 1. Lattice parameters a as a function of temperature for ZrNiSn and TiNiSn and their Ce alloys. The calculated $a(T)$ are shown as a solid lines. The thermal lattice expansion plots of the respective Ce alloys are normalized at $T = 300$ K to the lattice parameters of ZrNiSn and TiNiSn respectively.

present lattice parameters as a function of temperature for ZrNiSn, TiNiSn and their Ce alloys. The experimental data are compared with calculations of $a(T)$ derived from the Debye theory. The Debye temperatures for ZrNiSn and TiNiSn were taken from reference [9]. The lattice parameter of ZrNiSn markedly deviates from the calculated curve at $T < 200$ K. This result suggests a non-magnetic-type phase transition without any change in the crystal structure. We also observed the same abnormal behaviour of $a(T)$ for TiNiSn below $T = 150$ K. In reference [16] this abnormal change of a observed in ZrNiSn below $T = 100$ K was attributed to a spontaneous change of the degree of substitution between the Zr and Sn sublattices.

A small degree of replacement of Ti by trivalent Ce destroys this phase transition of the disorder–order type and leads to the characteristic $a(T)$ dependence predicted by the Debye lattice vibration model (figure 1). The lattice parameter of $Zr_{1-x}Ce_xNiSn$ alloys plotted as a function of T shows a small collapse below $T = 100$ K, which does not depend on the concentration of Ce impurities and could be attributed to crystal-field effects.

In figure 2 we show the temperature dependences of the intensities of (200) Bragg lines in ZrNiSn, TiNiSn and their Ce alloys. The continuous curves are calculated from the relation $I(T) = I_0 \exp(-B(T) \sin^2\theta/\lambda^2)$, where the Debye–Waller factor B was calculated using the Debye lattice vibration model. Both ZrNiSn and TiNiSn show a disagreement between the calculated and measured intensities, that can be attributed to a change of substitutional disorder. This abnormal behaviour in the $I(T)$ plots was only observed for those crystallographic planes which are occupied by the M = Zr or Ti and Sn atoms. The effect, however, was not measured

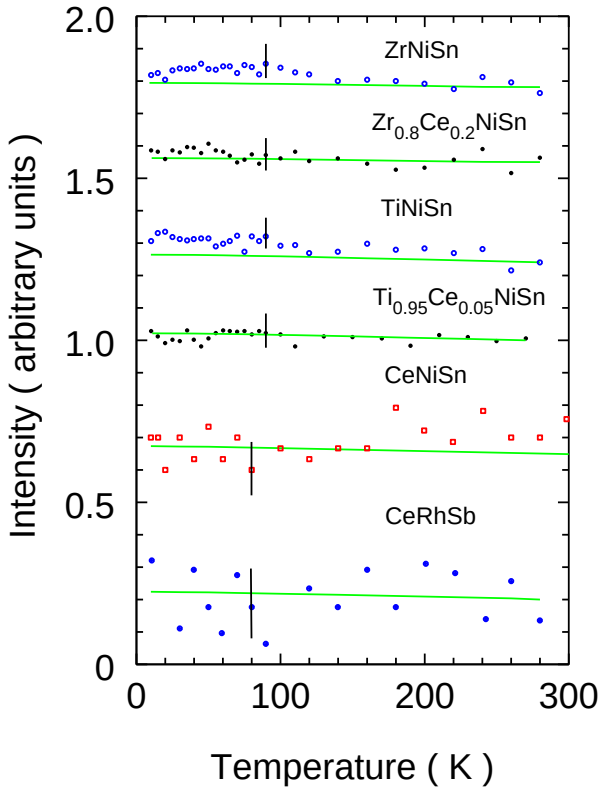

Figure 2. The intensities $I(T)/I(300\ \mathrm{K})$ of the (220) x-ray diffraction lines of the MNiSn-type alloys are compared with the calculated ones. A similar comparison is presented for the (220) Bragg's line for the orthorhombic CeNiSn and CeRhSb.

(This figure can be viewed in colour in the electronic version of the article; see `www.iop.org`)

for the samples with Ce impurities.

A second abnormal behaviour in the $a(T)$ plot was observed for ZrNiSn below 40 K. The lattice parameter has a minimum which is difficult to explain. The low-temperature increase of a correlates with the resistivity upturn, which was attributed in reference [15] to the transition from the quasimetallic to Mott's behaviour. The exponential form $\rho = \rho_0 \exp(T_0/T)^{1/4}$ (reference [17]) describes well the resistivity increase observed both in ZrNiSn and in TiNiSn at $T < 30$ K [15]; however, the reason suggested for the low-T resistivity upturn seems to us to be very questionable, if one considers that the low-temperature volume effect on ρ also mirrors the volume effect on the magnetic susceptibility χ [6]. However, we have no tenable reasons for suggesting e.g. breaking of the symmetry at $T = 40$ K, which could lead to gap formation, which probably is observed in the resistivity. A linear scaling of $a(T)$ with χT in figure 3 suggests the splitting of the volume effects and the weak magnetic properties of the ground state (a strongly enhanced Pauli paramagnet). The low-temperature volume effect in ZrNiSn is relatively small and it is not detected for isoelectronic TiNiSn. However, at $T < 40$ K TiNiSn still shows a linear dependence of $a(T)$ versus χT (figure 3) although there is a strong temperature dependence in its susceptibility. Moreover, the high-temperature slopes of $\Delta a/\Delta(\chi T)$ (figure 3) for the two alloys are almost the same [6].

The Kondo insulators CeNiSn and CeRhSb show volume abnormalities analogous to those

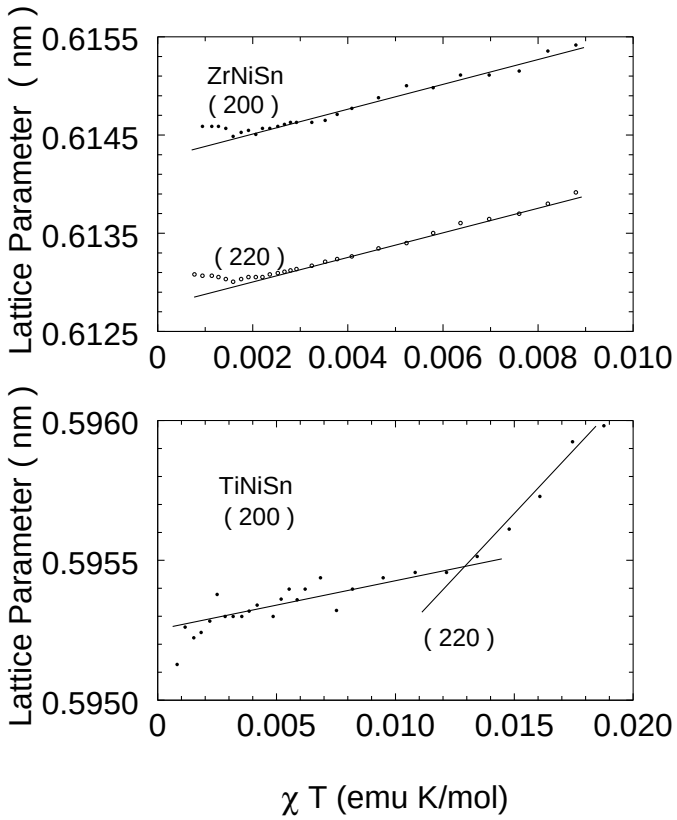

Figure 3. Lattice parameter a as a function of χT for ZrNiSn and TiNiSn.

of ZrNiSn or TiNiSn. In figure 4 we present the lattice parameters of CeNiSn and CeRhSb versus T. For both compounds the thermal expansion coefficients include the phonon and crystal-field effects. Moreover, the lattice parameter a in CeNiSn presents the phase transition at $T = 200$ K (without a change of the crystal structure) very much analogous to that observed for ZrNiSn or TiNiSn. This phase transition may be due to a spontaneous change in the substitution of the Ce and Sn sublattices. A small amount of La at the Ce positions destroys this transition and stabilizes the structure. The large difference between the Ce- and Sb-atom radii makes the probability of their mutual substitution small; therefore we did not observe any abnormal change of the lattice parameter a in CeRhSb.

For CeRhSb the lattice parameters a, b and c vary linearly with χT; however, for CeNiSn we observed two different linear relations for $a(T)$, $b(T)$ and $c(T)$ versus χT with a distinct intersection at about $T = 170$ K (figure 5). One can see similarities between figure 3 and figure 5. Excluding the Mott low-temperature region, ZrNiSn seems to be a good analogue for CeRhSb, while TiNiSn is a good one for CeNiSn. The volume effect in CeNiSn can also be enhanced by the Ce 4f and Sn 5p hybridization, which is strong in this compound [18]. The magnetic susceptibility of CeRhSb and CeNiSn is typical for cerium valence-fluctuation compounds. Recently, it has been analysed on the basis of the ionic two-level interconfiguration fluctuation (ICF) model proposed by Sales and Wohlleben [19]. In this model $\chi(T) = \chi_0 + nC/T + N\mu^2 n_{\mathrm{f}}^{\chi}/3k_B(T + T_{sf})$, the valence fraction $n_{\mathrm{f}}^{\chi}(T)$ is computed from Boltzmann statistics for $4\mathrm{f}^1$ and $4\mathrm{f}^0$ levels which are separated by an energy E_x. T_{sf} is

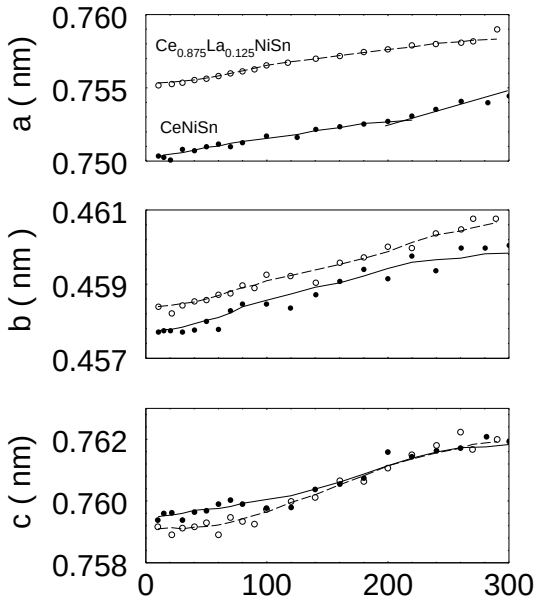

(a)

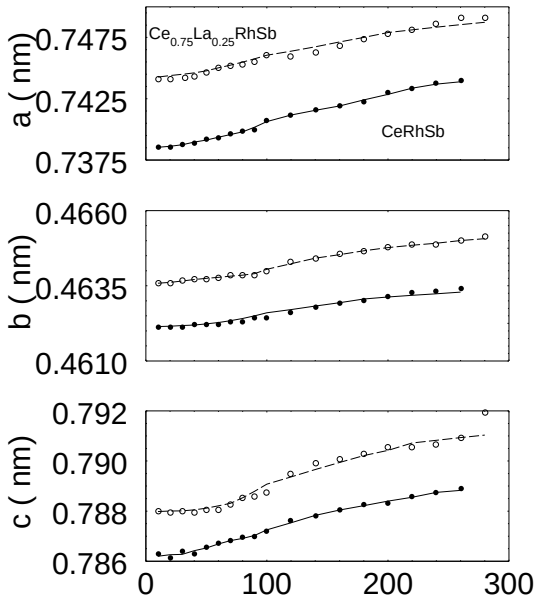

(b)

Figure 4. Lattice parameters versus T for: (a) CeNiSn and $Ce_{0.875}La_{0.125}NiSn$; (b) CeRhSb and $Ce_{0.75}La_{0.25}RhSb$.

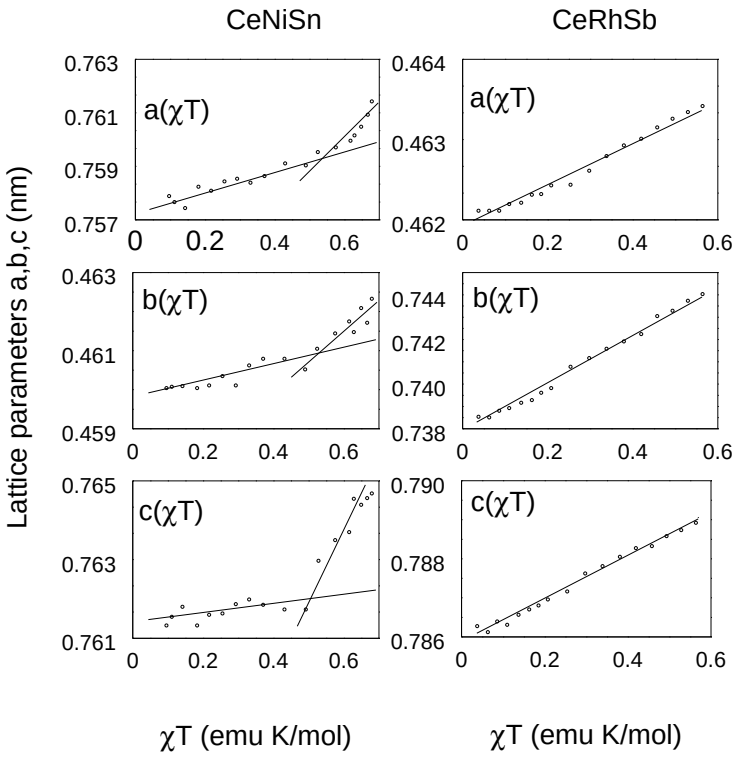

Figure 5. Lattice parameters of CeNiSn and CeRhSb as functions of χT.

the inverse of the valence-fluctuation lifetime, while a Curie–Weiss term nC/T explains the observed upturn in the susceptibility caused by a fraction n of the paramagnetic Ce impurities. However, a relatively large value of n (table 1; recently discussed in references [3,5,8]) cannot be responsible for the volume effect in CeNiSn at $T = 200$ K.

Table 1. The magnetic properties of CeNiSn and CeRhSb. The values of χ_0, n, T_{sf} and E_x/k_B are defined by fitting $\chi(T)$ to the experimental magnetic susceptibility data. n_{f}^{χ} is an occupation number obtained from the susceptibility on the basis of the ICF model. Δ is the hybridization constant.

	CeNiSn	CeRhSb
χ_0 in emu mol^{-1}	8.0×10^{-4}	7.4×10^{-4}
Impurity concentration n	0.06	0.02
T_{sf} in K	120	250
E_x in K	144	250
n_{f}^{χ} at $T = 300$ K	0.81	0.71
$n_{\mathrm{f}}^{\mathrm{XPS}} = 1 - I(\mathrm{f}^0)/(I(\mathrm{f}^0) + I(\mathrm{f}^1) + I(\mathrm{f}^2))$	0.95	0.86
Δ in meV	200	140

A 'Kondo insulator' has a non-magnetic ground state, an insulating gap and low-lying excitations which exhibit properties of strong correlation. These properties do not classify Kondo insulators as Mott or charge-transfer insulators, which generally have antiferromagnetic

ground states. We have argued above that the Zr and Ti semi-Heusler alloys and CeNiSn-type Kondo insulators have similar crystallographic properties. The ground states of CeNiSn and of TiNiSn are different; however, they can both be attributed to the vacancy bands. In TiNiSn and ZrNiSn, vacancy levels are located above the Fermi level and overlap with the conduction bands [10]. At low temperatures the enhancement of the effective mass can be deduced from the narrow band with a width of about a few hundred K due to the localization of the valence electrons in the ordered vacancy sublattice. The vacancy model could also explain the transition from the quasimetallic to Mott's behaviour observed in reference [15] for $T < 30$ K.

The effects of vacancies on Kondo insulators is quite different and has been discussed by Schlottmann *et al* [20]. A neutral charge substitution for Ce (e.g. with La) leads to a hole in the f states which is known as a Kondo hole. As was shown in reference [20], a finite concentration of Kondo holes generates a band in the gap that progressively smears the hybridization gap and also can lead to magnetic properties. There is an insulator–metal transition as a function of the Kondo-hole concentration which usually occurs at a critical concentration of about 10% [20]. It is generally believed that the hybridization between the 4f and the conduction electrons is responsible for the gap formation in Kondo insulators, except for SmB_6. In SmB_6 the hybridization gap model has been found inconsistent with the high-pressure resistivity and Hall-effect measurements [21] which suggest that it is a Mott–Hubbard insulator.

In the light of this consideration, we will discuss the abnormal volume behaviour observed in CeNiSn and CeRhSb at about $T = 40$ K. Recently, Nolten *et al* [22] reported that below $T = 38$ K, the coefficient of the volume expansion of CeRhSb has a distinct contribution which coincides with a change in the slope of the electrical resistivity; however, no corresponding anomaly has been found in the specific heat data published so far. The magnetic contribution to the specific heat c_m/T has only shown a just visible change at $T < 38$ K [23]. Nevertheless, the nature of this contribution in $\alpha(T)$ was not discussed in reference [22]. Note that several experiments carried out independently have indicated this resistivity change below $T = 40$ K either for CeRhSb or CeNiSn (e.g. references [2,24,25]). This abnormal change of the thermal volume expansion coefficient α seems to be analogous to that observed below $T = 40$ K in ZrNiSn. Therefore, we believe that the same features are responsible for the volume and resistivity anomalies observed at $T < 40$ K in both the semi-Heusler alloys of the ZrNiSn type and the CeNiSn-type Kondo insulators. In addition, the Mott-type behaviour, if it is indeed due to the abnormal resistivity increase in ZrNiSn and TiNiSn at $T = 40$ K, can also be attributed to the ground state of the Kondo-insulator-type alloys. In this sense, however, a large competition of the band hybridization and the Kondo-type interactions can disturb the Mott–Hubbard insulator state.

We again cite SmB_6 as an example of a striking parallel to Mott–Hubbard insulators such as V_2O_3 [21]. Spałek *et al* [26] have presented the diagram on the T–U/W plane of possible metal–insulator transitions, where U represents the intra-atomic Coulomb repulsion and W is the bandwidth. Near the tricritical point on this plot, it is possible to observe the transition from the paramagnetic metal to the paramagnetic insulator; however, the low-temperature ground state should be antiferromagnetic. Moreover, for Kondo insulators this state is not seen in the most recent experiments (e.g. in references [27]), but some experiments (e.g. in references [28, 29]) suggest low-temperature antiferromagnetic correlations.

3.2. Electronic structure

Recently, we presented the Ce 3d XP spectra for CeNiSn and CeRhSb [5, 8], which give information about the 4f-shell configuration and hybridization strength. On the basis of the Gunnarsson and Schönhammer theoretical model [30], three final-state contributions: f^0, f^1

and f^2 of the Ce 3d XP spectra indicate an f occupation number $n_f^{XPS} < 1$ and a hybridization width Δ of about 200 meV (table 1). This analysis showed visible hybridization effects in the valence bands and good correlation with the susceptibility results (table 1).

Ultraviolet photoemission spectroscopy is a powerful technique for studying the electronic properties of solids near the Fermi level. Such studies of polycrystalline materials can be used to determine the density of states (DOS) of the alloy and, more interestingly, can be used to determine the contribution to the valence bands of the constituent elements. Since the cross-section of s states is comparatively low for all the elements in MNiSn and MRhSb samples, the photoemission spectra in figures 6–13 are dominated by transitions from the d bands (figure 14 and reference [31]). We compare the photoemission spectra for $h\nu = 21.2$ (He I), 40.8 (He II) and 1486.6 eV (Al Kα) with the calculations. All the photoemission spectra are subtracted from the background which has been calculated using the well established Tougaard algorithms [32]. The spectra are detected at room temperature, while the calculations have been done for the ground state at $T = 0$, and the calculated gap size in Ce alloys is considerably smaller than the standard resolution of the measured valence band XP and UP spectra. This makes discussion of the Kondo-insulator behaviour impossible, even through the recorded spectra are qualitatively similar to the convoluted DOS curves. The spectra demonstrate a valence band that has a major peak that is mainly due to the d states located near the Fermi level. The second peak centred at about 8 eV is observed for ZrNiSn and TiNiSn alloys in the 40.8 and 21.2 eV UP spectra, but for the Ce Kondo insulators it is only just detectable. The intensity profile of the 8 eV peak shows a strong energy dependence for TiNiSn and ZrNiSn, whereas for CeNiSn it has almost the same shape at the different photon energies. This peak is well known to be a resonant satellite for Ni [33–35]. The strong intensity enhancement at resonance is due to the influence of two excitation channels. One channel involves the excitation of a

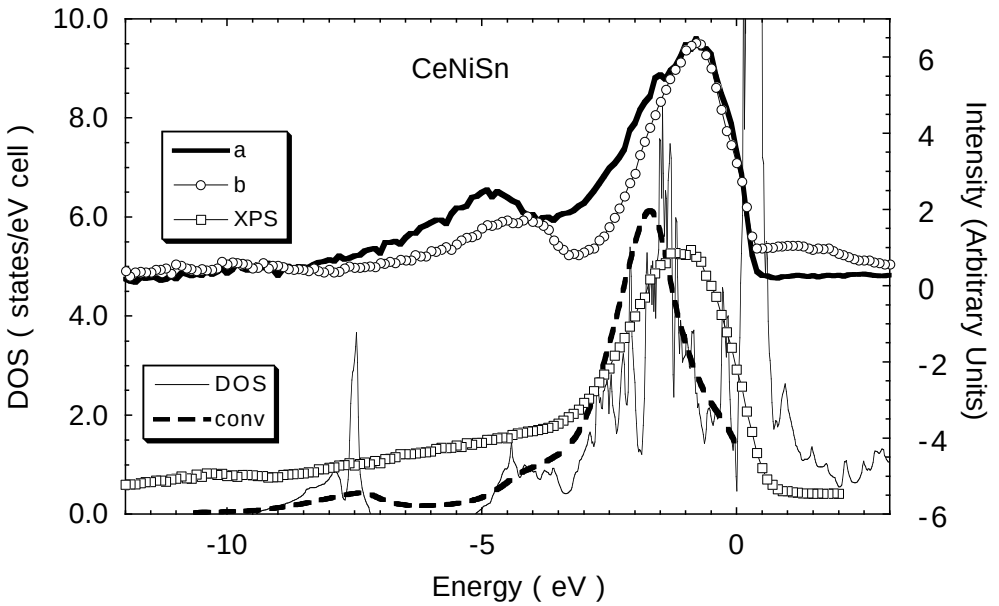

Figure 6. The DOS (solid thin line) and the DOS convoluted by Lorentzians of the half-width 0.4 eV and taking into account appropriate cross-sections for bands with different l-symmetry (dashed line) are compared with the XPS valence bands (squares) and with the measured $h\nu = 21.2$ (a) and 40.8 eV (b) UP spectra.

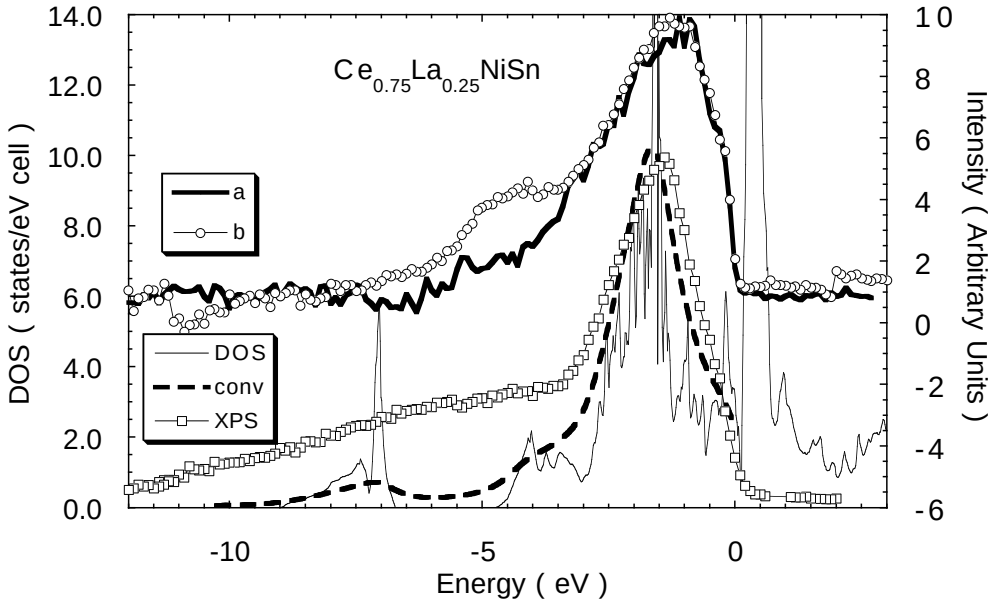

Figure 7. The total DOS compared with the $h\nu = 21.2$, 40.8 and 1486.6 eV photoemission spectra. The details are given in the description of figure 6.

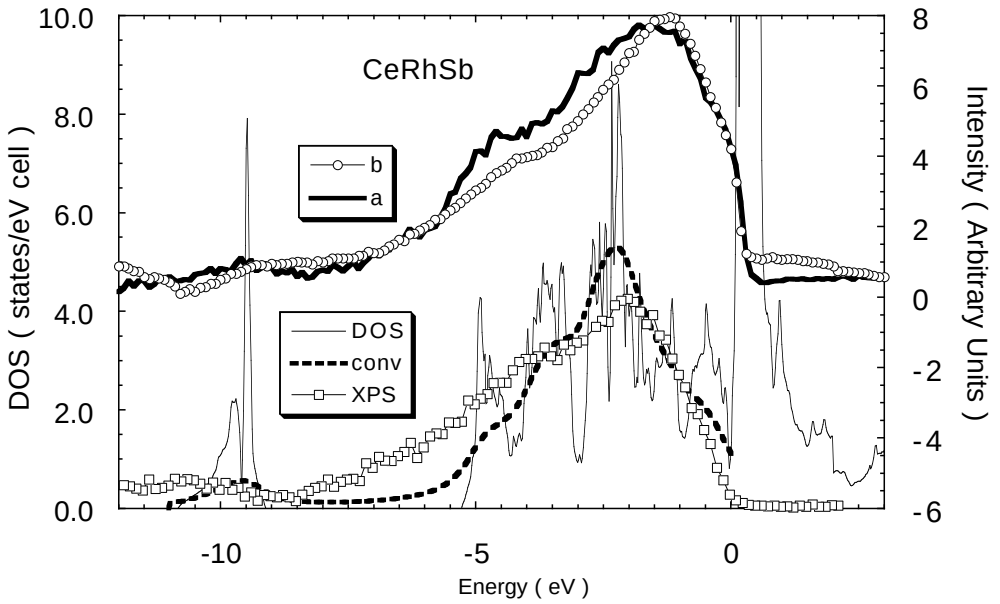

Figure 8. The total DOS compared with the $h\nu = 21.2$, 40.8 and 1486.6 eV photoemission spectra. The details are given in the description of figure 6.

core-level electron (3p–3d) followed by a coherent Auger-type decay leaving two holes at one site. The same final state can be obtained by a shake-up process. In Ni, the satellite shows considerable intensity even far from resonance (e.g. at XPS energies [36]); however, at the

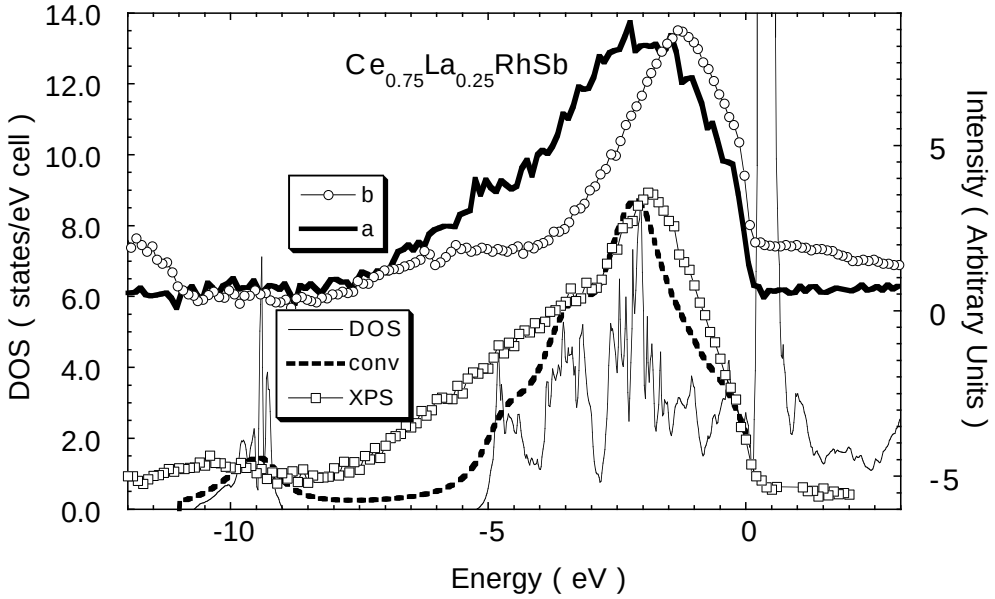

Figure 9. The total DOS compared with the $h\nu = 21.2$, 40.8 and 1486.6 eV photoemission spectra. The details are given in the description of figure 6.

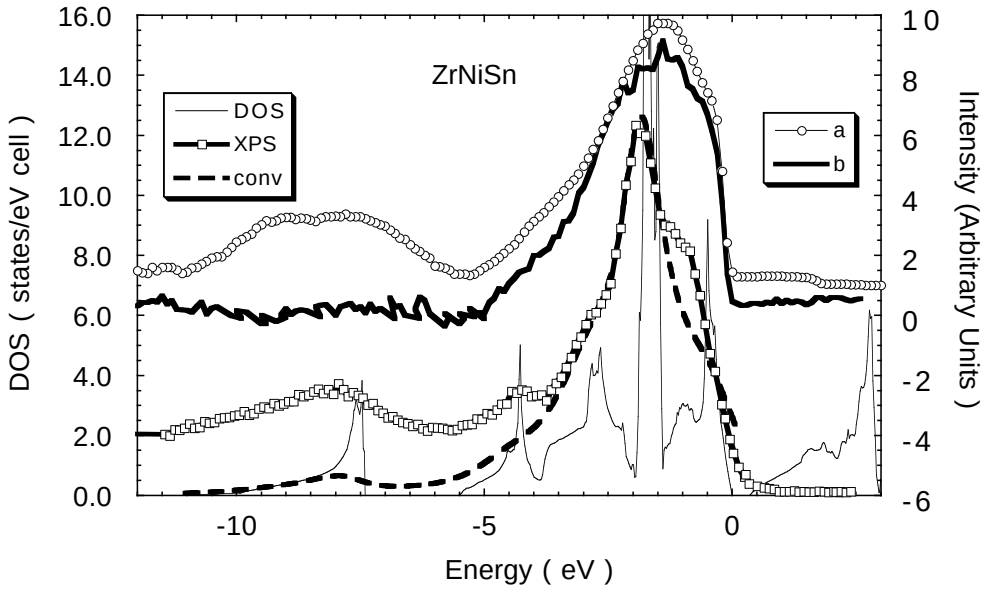

Figure 10. The total DOS compared with the $h\nu = 21.2$, 40.8 and 1486.6 eV photoemission spectra. The details are given in the description of figure 6.

resonance threshold, a 3p–3d transition leads to a strong enhancement of the satellite. In this experiment we are far from the resonance; therefore, the reason for the strong enhancement in the satellite intensity in the 40.8 eV spectrum of TiNiSn in comparison with CeNiSn seems to be more complicated. It also cannot be explained on the basis of the calculated one-electron

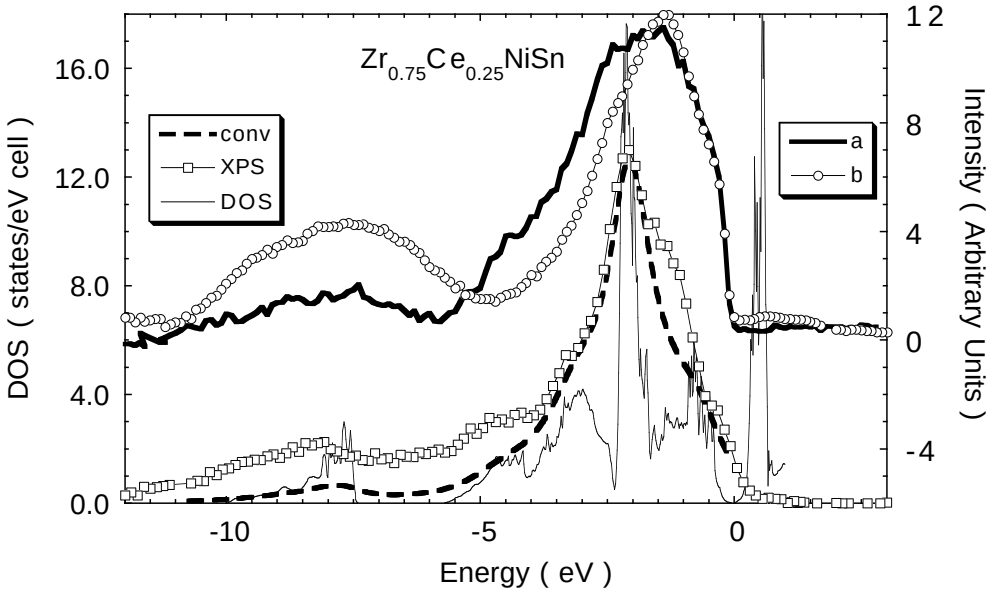

Figure 11. The total DOS compared with the $h\nu = 21.2$, 40.8 and 1486.6 eV photoemission spectra. The details are given in the description of figure 6.

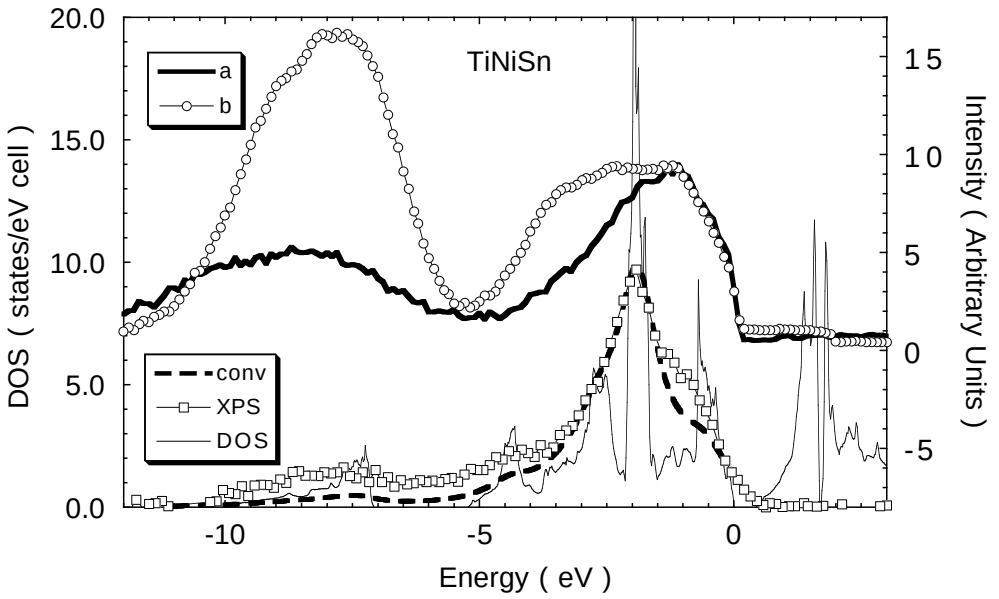

Figure 12. The total DOS compared with the $h\nu = 21.2$, 40.8 and 1486.6 eV photoemission spectra. The details are given in the description of figure 6.

ground-state bands. We believe that the strong peak in the UP spectra 8 eV below ϵ_F, which is visible for TiNiSn and ZrNiSn but not for the Ce alloys, also manifests the d character of the valence bands of Ti or Zr due to the many-body effects. The final state that has two 3d holes is the same as that produced by $L_3M_{45}M_{45}$ Auger transition. In figure 15 we present the LMM

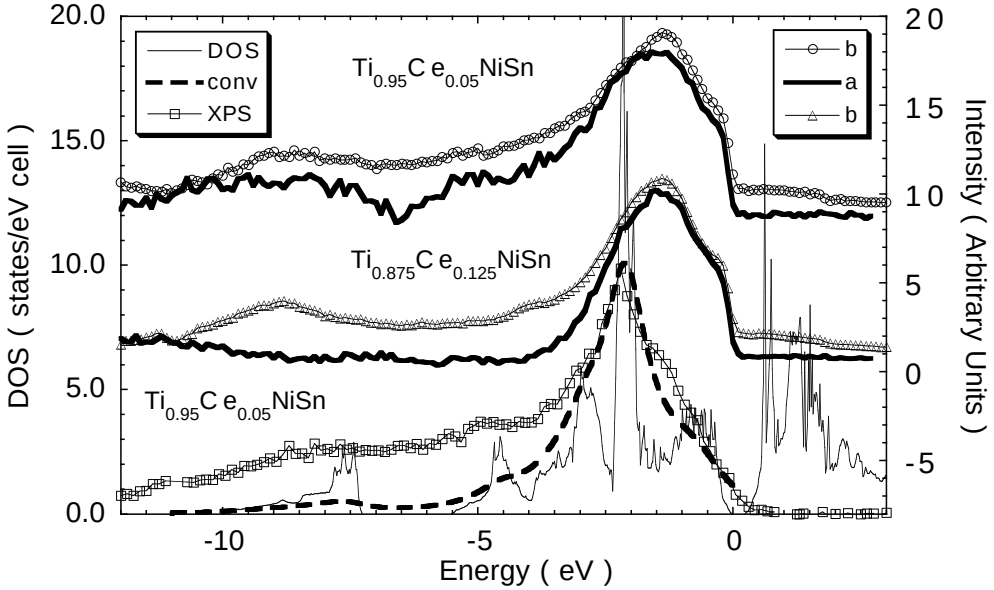

Figure 13. The total DOS compared with the $h\nu = 21.2$, 40.8 and 1486.6 eV photoemission spectra. The details are given in the description of figure 6.

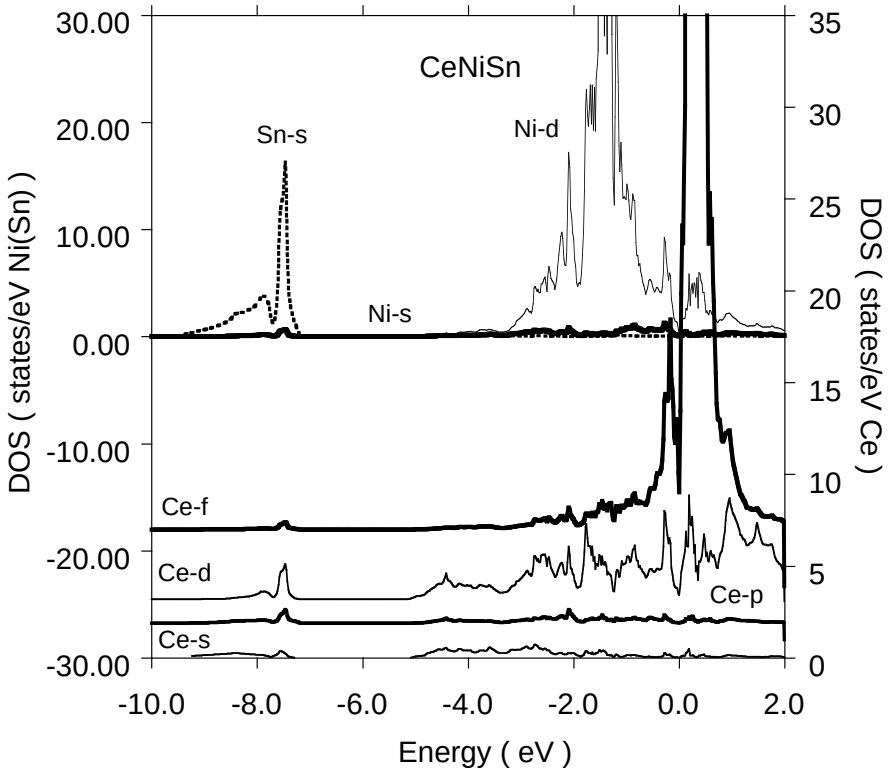

Figure 14. The partial DOS for CeNiSn.

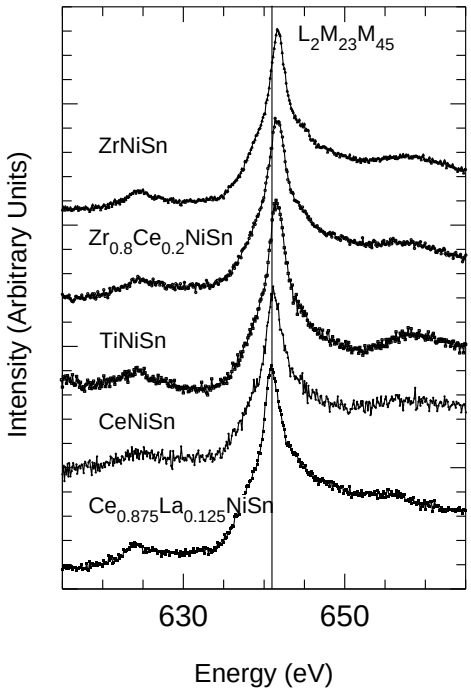

Figure 15. Ni LMM Auger spectra. The perpendicular line indicates the energy of this line for pure Ni metal.

Auger spectra of MNiSn compounds. All the spectra show one dominant line characteristic for the transition d-type elements. However, we observe an energy shift of about 0.7 eV higher kinetic energy E_k in the Zr and Ti alloy spectra in relation to those for the CeNiSn sample. The Sn MNN spectra presented in figure 16 are almost identical and are also shifted to higher E_k with respect to those for pure Sn. These shifts suggest strong Ce (or M) 4f (d)–Sn d, p hybridization, that is stronger than the Ce 4d–Ni 3d hybridization. The hybridization effect in the valence band between the d bands seems to be very important in ZrNiSn and TiNiSn. Recently, we have presented the XPS binding energies of the maxima of the core levels for a series of Zr Heusler and semi-Heusler alloys [6]. A shift of about 1 eV in the XPS lines indicated the strong redistribution of charge in these alloys due to intersite hybridization effects. The largest effect was found for the Zr and Sn atoms, in agreement with Auger results.

4. Conclusions

The calculations of the electronic structure of the MNiSn-type alloys with the M element tetravalent (Zr, Ti) and of the CeNiSn-type Kondo insulators showed similar energy distributions of the densities of states. The semiconducting gap was calculated for MNiSn, whereas for CeNiSn and CeRhSb at the Fermi level there is a narrow pseudogap. For both systems the second gap is calculated to be a few eV below the Fermi level. At about 8 eV, just below the second gap, the d states give the signals in the ultraviolet photoemission and x-ray photoelectron spectra which are characteristic for TiNiSn and ZrNiSn in the 40.8 eV UP spectrum.

Very similar band properties, such as strong hybridization, the gap formation at the Fermi energy and the second gap in the middle of the valence band, and the almost identical shapes

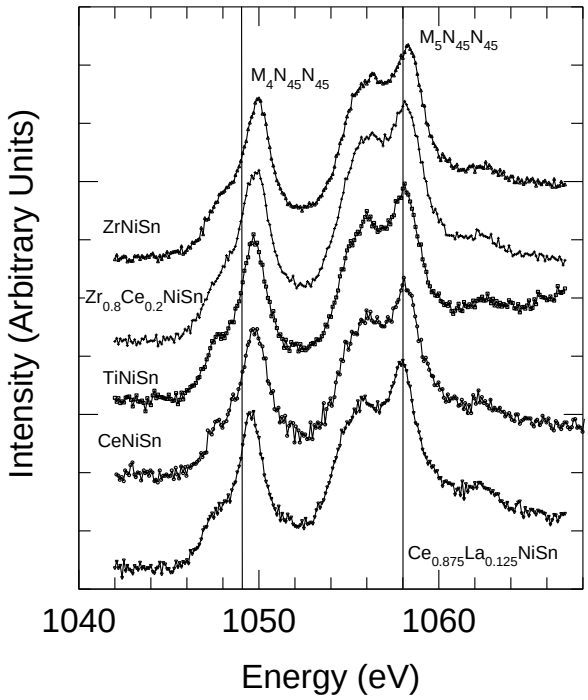

Figure 16. Sn MNN Auger spectra. The perpendicular lines indicate the energies of the appropriate lines for pure Sn metal.

of the photoemission spectra allowed us to classify both MNiSn and CeNiSn into the common group of intermetallics with the hybridization gap at the Fermi energy.

The low-temperature anomalies due to the lattice ordering we discussed as a characteristic either for the MNiSn semi-Heusler alloys with the M element tetravalent or the CeNiSn-type Kondo insulators. As the lattice becomes more ordered, these anomalies increase in number. At about $T = 40$ K we observed in the thermal volume expansion the abnormal behaviour specific to ZrNiSn-type and CeNiSn-type alloys. The volume effects correlate with the abnormal increase of the resistivities.

Acknowledgments

We are most grateful to Joanna Kapusta for her help in the x-ray diffraction experiment carried out at low temperatures. One of us (AJ) thanks the State Committee for Scientific Research for financial support (Project No P03B02715). The calculations were made at the Supercomputing and Networking Centre of Poznań.

References

[1] Takabatake T, Nakazawa Y and Ishikawa M 1987 *Japan. J. Appl. Phys. Suppl.* **26** 547
[2] Takabatake T, Teshima F, Fujii H, Nishigori S, Suzuki T, Fujita T, Yamaguchi Y, Sakurai J and Jaccard D 1990 *Phys. Rev.* B **41** 9607
[3] Malik S K and Adroja D T 1991 *Phys. Rev.* B **43** 6277
[4] Hundley M F, Confield P C, Thompson J D and Fisk Z 1990 *Phys. Rev.* B **42** 6842

[5] Ślebarski A, Jezierski A, Zygmunt A, Mähl S and Neumann M 1998 *Phys. Rev.* B **58** 13 498
[6] Ślebarski A, Jezierski A, Zygmunt A, Mähl S and Neumann M 1998 *Phys. Rev.* B **57** 9544
[7] Ślebarski A, Jezierski A, Lütkehoff S and Neumann M 1998 *Phys. Rev.* B **57** 6408
[8] Ślebarski A, Jezierski A, Zygmunt A, Mähl S, Neumann M and Borstel G 1996 *Phys. Rev.* B **54** 13 551
[9] Aliev F G, Kozyrkov V V, Moshchalkov V V, Skolozdra R V and Durczewski K 1990 *Z. Phys.* B **80** 353
[10] Aliev F G 1991 *Physica* B **171** 199
[11] Baer Y, Busch G and Cohn P 1975 *Rev. Sci. Instrum.* **46** 466
[12] Andersen O K and Jepsen O 1984 *Phys. Rev. Lett.* **53** 2572
Andersen O K, Jepsen O and Sob M 1987 *Electronic Structure and Its Applications* ed M Yussouff (Berlin: Springer) p 2
[13] von Barth U and Hedin L 1972 *J. Phys. C: Solid State Phys.* **5** 1629
[14] Hu C D and Langreth D C 1985 *Phys. Scr.* **32** 391
[15] Aliev F G, Brandt H B, Kozyrkov V V, Moshchalkov V V, Skolozdra R V, Stadnyk Yu V and Pecharskii V V 1987 *Pis. Zh. Eksp. Teor. Fiz.* **45** 535
[16] Aliev F G, Brandt N B, Moshchalkov V V, Kozyrkov V V, Skolozdra R V and Belogorokhov A I 1989 *Z. Phys.* B **75** 167
[17] Mott N F 1971 *Phil. Mag.* **24** 911
[18] Nohara S, Namatame H, Fujimori A and Takabatake T 1993 *Phys. Rev.* B **47** 1754
[19] Sales B C and Wohlleben D 1975 *Phys. Rev. Lett.* **35** 1240
[20] Schlottmann P 1996 *Phys. Rev.* B **54** 12 324
[21] Cooley J F, Aronson M C, Fisk Z and Confield P C 1995 *Phys. Rev. Lett.* **74** 1629
[22] Nolten A J, de Visser A, Kayzel F E, Franse J J M, Tanaka H and Takabatake T 1995 *Physica* B **206+207** 825
[23] Takabatake T, Nakamoto G, Tanaka H, Bando Y, Fujii H, Nishigori S, Goshima H, Suzuki T, Fujita T, Oguro J, Hiraoka T and Malik S K 1994 *Physica* B **199+200** 457
[24] Uwatoko Y, Ishii T, Oomi G, Takahasi H, Mori N, Thompson J D, Shero J L, Madru D and Fisk Z 1996 *J. Phys. Soc. Japan* **65** 27
[25] Malik S, Menon L, Pecharsky V K and Gschneidner K A Jr 1997 *Phys. Rev.* B **55** 11 471
[26] Spałek J, Datta A and Honig J M 1987 *Phys. Rev. Lett.* **59** 728
Carter S A, Yang J, Rosenbaum T F, Spałek J and Honig J M 1991 *Phys. Rev.* B **43** 607
[27] Kyogaku M, Kitaoka Y, Nakamura H, Asayama K, Takabatake T, Teshima F and Fujii H 1990 *J. Phys. Soc. Japan* **59** 1728
Kyogaku M, Kitaoka Y, Nakamura H, Asayama K, Takabatake T, Teshima F and Fujii H 1991 *Physica* B **171** 235
[28] Kalvins G M, Kratzer A, Wappling R, Takabatake T, Nakamoto G, Fuji H, Kiefl R F and Kreitzmann S R 1995 *Physica* B **206+207** 807
[29] Mason T E, Aeppli G, Ramirez A P, Clausen K N, Broholm C, Stücheli N, Bucher E and Palstra T T M 1992 *Phys. Rev. Lett.* **69** 490
[30] Gunnarsson O and Schönhammer K 1983 *Phys. Rev.* B **28** 4315
[31] Yeh J J and Lindau I 1985 *At Data Nucl. Data Tables* **32** 1
[32] Tougaard S and Sigmund P 1982 *Phys. Rev.* B **25** 4452
[33] Hüfner S and Wertheim G 1975 *Phys. Lett.* A **51** 299
Hüfner S and Wertheim G 1975 *Phys. Lett.* A **51** 301
[34] Hüfner S, Hulliger F, Osterwalder J and Riesterer T 1984 *Solid State Commun.* **50** 83
[35] Thuller M R, Benbow R L and Hurych Z 1983 *Phys. Rev.* B **27** 2082
[36] Penn D R 1979 *Phys. Rev. Lett.* **42** 673